

Semantic Communication and Control Co-Design for Multi-Objective Correlated Dynamics

Abanoub M. Girgis, *Student Member, IEEE*, Hyowoon Seo, *Member, IEEE*, and Mehdi Bennis, *Fellow, IEEE*

Abstract—This letter introduces a machine-learning approach to learning the semantic dynamics of correlated systems with different control rules and dynamics. By leveraging the Koopman operator in an autoencoder (AE) framework, the system’s state evolution is linearized in the latent space using a dynamic semantic Koopman (DSK) model, capturing the baseline semantic dynamics. Signal temporal logic (STL) is incorporated through a logical semantic Koopman (LSK) model to encode system-specific control rules. These models form the proposed logical Koopman AE framework that reduces communication costs while improving state prediction accuracy and control performance, showing a 91.65% reduction in communication samples and significant performance gains in simulation.

Index Terms—6G, signal temporal logic, predictive control, communication-control co-design.

I. INTRODUCTION

THE rapid advancement of communication and control systems is foundational for advancing modern sixth-generation (6G) communication applications [1], [2]. However, these systems often operate in isolation, limiting scalability and complicating stability in distributed environments with constrained communication. To overcome these challenges, communication and control co-design (CoCoCo) approaches optimize communication resources without compromising control performance. For example, existing approaches focus on control scheduling and resource allocation, adapting to channel and control states for improved system stability [3]–[5]. While effective, these strategies prioritize data exchange over extracting meaningful dynamics, a crucial factor in ensuring control effectiveness.

In the meantime, recent machine learning (ML) advancements have introduced semantic and goal-oriented communication, particularly in beyond fifth generation (B5G) and 6G networks [6]–[8]. Semantic communication, aligned with CoCoCo’s objective, enhances communication efficiency and effectiveness by transmitting only task-relevant information. Unlike traditional methods, it leverages ML to extract and convey meaningful data rather than raw information. This approach suggests that so-called *semantic CoCoCo* will play a pivotal role in future systems, though challenges in communication cost, stability, and scalability across different systems persist [9]. While most semantic CoCoCo approaches rely on ML models that require significant training data, correlated control systems can exploit shared semantic structure, using a reference system’s dynamics. In contrast, systems with distinct behaviors often need independent models, posing scalability challenges.

A. M. Girgis and M. Bennis are with the Centre for Wireless Communications, University of Oulu, Oulu 90014, Finland (e-mail: abanoub.pipaoy@oulu.fi; mehdi.bennis@oulu.fi).

H. Seo is with the Department of Electronics and Communications Engineering, Kwangwoon University, Seoul, South Korea (e-mail: hyowoon-seo@kw.ac.kr).

Building on our preliminary work in [9], which demonstrated the effectiveness of controlling multi-objective identical systems, this paper addresses a new challenge: controlling *multi-objective distinct control systems*. These are distinct yet correlated mixed logical dynamical (MLD) systems, each with unique objectives and dynamics, but sharing baseline dynamics. These systems differ primarily in control rules and dynamic variations. We leverage a Koopman operator theory [10] within an AE architecture to linearize system state evolution in the latent space using a dynamic semantic Koopman (DSK) model, which captures the baseline semantic structure. To handle the system-specific variations, we incorporate signal temporal logic (STL) [11] into the latent space through the logical semantic Koopman (LSK) model to encode the system-specific control rules. Pre-training the encoder-decoder enables the AE to adapt to dynamic variations. Composing these models forms a novel semantic CoCoCo approach proposed in this letter as the logical Koopman AE framework.

To train the logical Koopman AE across multiple systems, we first train the encoder, decoder, and DSK model on a reference system devoid of control rules and dynamics variations, ensuring their applicability across different systems. Next, each system’s LSK model is trained by optimizing a loss function based on the local control rule. This approach significantly reduces communication costs associated with training each system’s dynamics, effectively addressing scalability without compromising control performance. Simulation on five distinct inverted cart-pole systems shows that our proposed framework yields a 75.78% improvement in average state prediction capabilities while reducing communication samples by 91.65% and improving the control performance by 92.91% at a 15 dB signal-to-noise ratio (SNR) and two-dimensional state representations.

II. PRELIMINARIES

A. System Model

Consider controlling multi-objective distinct correlated control systems composed of plants, sensors, and remote controllers, as depicted in Fig. 1. The set of plants is denoted by \mathcal{I} , where each plant represents a non-linear dynamic *process* controlled by an *actuator*, with sensors sampling the process state. These sampled states are sent to a remote controller with high computational power, calculating the target control commands. The commands are then transmitted back to the actuators to drive the process to the desired behavior. The sensors and actuators are co-located and share a transceiver for wireless communication, while the remote controller communicates with the sensors via wireless channels. Each plant follows distinct *control rules* to meet objectives like stability and safety. Further details on the control and communication systems are provided next.

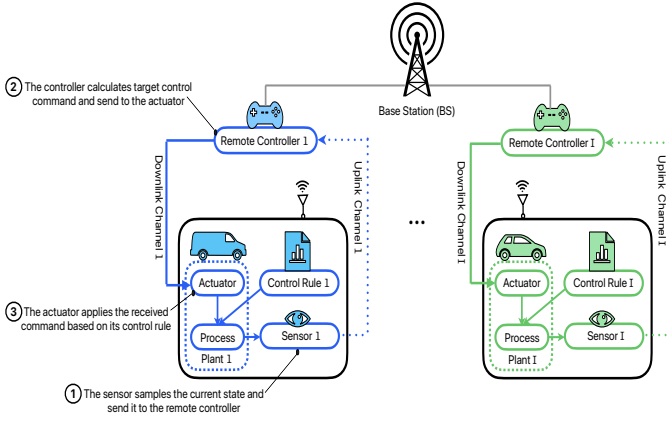


Fig. 1. An illustration of the multi-objective distinct control systems.

1) *Control System*: Each plant's sensor samples its p -dimensional state at a sampling rate τ_o and transmits these to the remote controller over a wireless channel. For plant $i \in \mathcal{I}$, the state at time $t = k\tau_o$ is given by $\mathbf{x}_{i,k} \in \mathbb{R}^p$. Upon receiving $\mathbf{x}_{i,k}$, the remote controller computes an optimal control command $\mathbf{u}_{i,k} \in \mathbb{R}^q$ and sends it to the actuator, which then influences the plant's state. The process state evolves as a control-affine non-linear dynamic system as [12]

$$\mathbf{x}_{i,k+1} = \mathbf{f}_{\varphi_i}^s(\mathbf{x}_{i,k}) + \mathbf{F}_{\varphi_i}^u(\mathbf{x}_{i,k})\mathbf{u}_{i,k} + \mathbf{n}_{s,k}, \quad (1)$$

under given control rules φ_i , where $\mathbf{n}_{s,k} \in \mathbb{R}^p$ is system noise, modeled as independent and identically distributed (i.i.d.) Gaussian random vector. $\mathbf{f}_{\varphi_i}^s$ represents the non-linear state transition function and $\mathbf{F}_{\varphi_i}^u$ is the state-dependent control function, both are subject to predefined control rules φ_i . Each control rule, φ_i , will be formalized as an STL formula, translating natural language rules into a mathematical format. This concept and its integration into the logical Koopman AE architecture are further discussed in Section III.

2) *Wireless Communication*: Each plant communicates with the remote controller using a dedicated orthogonal channel. Both uplink (sensor-to-controller) and downlink (controller-to-actuator) transmissions share the same channel, alternating via a time-division duplex. Channel reciprocity ensures consistent transmission power P_i for both directions. Wireless channels are modeled using path loss and Rayleigh fading, with path loss defined as

$$\text{PL}_{\text{dB}}(D) = \text{PL}_{\text{dB}}(D_0) + 10\eta \log_{10} \left(\frac{D}{D_0} \right), \quad (2)$$

where D is the transmitter-receiver distance, $\text{PL}_{\text{dB}}(D_0)$ is the path loss at the reference distance D_0 , and $\eta \geq 2$ is the path loss exponent. The received SNR for plant i at time k is expressed as

$$\gamma_{i,k} = 10^{-\frac{\text{PL}_{\text{dB}}(D_0)}{10}} \frac{P_i |H_{i,k}|^2}{N_c} \left(\frac{D_0}{D} \right)^\eta, \quad (3)$$

where $H_{i,k}$ is the Rayleigh fading channel gain, and N_c is the power of additive white Gaussian noise. The channel capacity for plant i at time k is expressed as

$$R_{i,k} = B \log_2(1 + \gamma_{i,k}), \quad (4)$$

with the outage probability given by

$$\epsilon_{i,k} = 1 - \exp \left[-10^{\frac{\text{PL}_{\text{dB}}(D_0)}{10}} \frac{N_c D^\eta}{P_i} \left(2^{\frac{R}{W}} - 1 \right) \right]. \quad (5)$$

where B is the transmission bandwidth and \bar{R} is the target transmission rate. Minimizing the outage probability necessitates designing control systems to operate at reduced communication overhead.

B. Background Principles

The Koopman operator provides a linear representation of non-linear dynamics, enabling efficient state prediction for closed-loop control while reducing communication overhead. STL translates knowledge-based control rules into a formal mathematical framework. Brief overviews of both concepts are provided next.

1) *Koopman Operator*: Consider a real-valued measurement function $\psi : \mathbb{R}^P \rightarrow \mathbb{R}$, termed as an observable, residing within an infinite-dimensional Hilbert space. The Koopman operator \mathcal{K} , a linear operator on this space, evolves the observable such that [13]

$$\psi(\mathbf{x}_{i,k+1}) = \mathcal{K}\psi(\mathbf{x}_{i,k}). \quad (6)$$

The Koopman operator linearizes non-linear dynamics in observable space but operates in an infinite-dimensional space, posing challenges. To address this, we identify an invariant subspace spanned by Koopman eigenfunctions $\psi_1, \psi_2, \dots, \psi_d$, where d is a finite positive integer, allowing for a finite-dimensional representation. Applying the Koopman operator to this subspace keeps the system in this subspace. Leveraging this linearity structure and linearly embedding control commands within observable space, we derive a global linear approximation of non-linear dynamics in (1) as [14]

$$\Psi(\mathbf{x}_{i,k+1}) = \mathbf{K}_A \Psi(\mathbf{x}_{i,k}) + \mathbf{K}_B \mathbf{u}_{i,k}, \quad (7)$$

where $\Psi(\cdot) \in \mathbb{R}^d$ is a vector of Koopman eigenfunctions, $\mathbf{K}_A \in \mathbb{R}^{d \times d}$ is the state-based transition Koopman matrix, and $\mathbf{K}_B \in \mathbb{R}^{d \times q}$ is the control-based Koopman matrix. However, discovering Koopman eigenfunctions from finite data remains challenging, so we adopt an AE-based deep learning approach to address this, as detailed later.

2) *Signal Temporal Logic*: STL is a formal language for analyzing and interpreting discrete-time signals from control systems [15]. STL defines control rules over predicates, such as $\mu_c := \mathbf{x}_i(p) < c$, where c is a scalar. The syntax of an STL formula is given by

$$\varphi := \mu_c \mid \varphi \wedge \vartheta \mid \square_{[a,b]} \varphi, \quad (8)$$

where $a, b \in \mathbb{Z}_+$ is finite discrete-time bounds, with $0 \leq a < b$, and φ and ϑ are STL formulas. \mid (pipe symbol) separates between STL formulas, \wedge (and) is boolean operator, and \square (always) is temporal operator.

A timed trace signal s_i records ordered sequence system state variables with timestamps. The satisfaction of an STL formula φ by a timed trace signal $s_{i,k}$ is quantified by the robustness function ρ , which measures how strongly the signal satisfies or violates the formula: [15]

$$\begin{aligned} \rho(s_{i,k}, \mu_c) &= c - \mathbf{x}_i(p) \\ \rho(s_{i,k}, \varphi \wedge \vartheta) &= \min(\rho(s_{i,k}, \varphi), \rho(s_{i,k}, \vartheta)) \\ \rho(s_{i,k}, \square_{[a,b]} \varphi) &= \min_{k' \in [k+a, k+b]} \rho(s_{i,k'}, \varphi). \end{aligned} \quad (9)$$

The robustness function maps a timed trace and STL formula to a real value: positive for satisfaction and negative for violation. Using a parse tree for STL formulas, we generate a directed acyclic graph (DAG) to compute the robustness

efficiently, with each sub-graph representing a node in the STL formula's operation sequence [9], [11]. This resulting computation graph reflects the robustness of STL formulas as described in (9).

III. LOGICAL KOOPMAN AUTOENCODER

This section introduces a novel semantic CoCoCo for controlling multi-objective distinct control systems, utilizing a logical Koopman AE inspired by the adapter technique in [16], which adapts a pre-trained model to new tasks without full retraining. In this framework, the Koopman model incorporates a trainable LSK model while keeping the DSK model frozen. The architecture consists of an encoder, a decoder, and a Koopman model with state and action components. The Koopman model shown in Fig. 2 is divided into four parts: two for the DSK model (state and action matrices) and two for the LSK model (state and action matrices), which govern the linear state evolution based on control rules. Training occurs in three phases: first, the encoder, decoder, and DSK model are trained on a reference system, then transferred to other systems where the LSK model is fine-tuned based on specific control rules. Finally, the systems are monitored remotely using linear predictions through the logical Koopman AE.

A. Dynamic Semantic Koopman Model

In the first phase of our remote control approach, a reference plant with simple dynamics and no specific control rule (denoted as $\varphi_i := \text{NULL}$) is selected as a benchmark. Here, we aim to optimize the encoder $\Psi(\cdot)$, decoder $\Psi^{-1}(\cdot)$, and DSK model, represented by matrices \mathbf{D}_A and \mathbf{D}_B . The optimization problem is formulated as

$$\arg \min_{\mathbf{D}_A, \mathbf{D}_B, \Psi, \Psi^{-1}} \frac{1}{K_s} \sum_{k=1}^{K_s} \|\mathbf{x}_{i,k} - \Psi^{-1}(\mathbf{D}_A \mathbf{z}_{i,k} + \mathbf{D}_B \mathbf{u}_{i,k})\|_2^2, \quad (10)$$

where $\mathbf{z}_{i,k} = \Psi(\mathbf{x}_{i,k})$ is the state representations of plant i at time k . Due to the complexity of obtaining an analytical solution of (10) for long-term prediction, we leverage deep learning and define three loss functions defined as.

- 1) A *reconstruction loss* (\mathcal{L}_1) ensures accurate reconstruction of the system states and is defined as follows.

$$\mathcal{L}_1 = \frac{1}{K_s} \sum_{k=1}^{K_s} \|\mathbf{x}_{i,k} - \Psi^{-1}(\mathbf{z}_{i,k})\|_2^2, \quad (11)$$

where K_s is the number of system states observed in the first phase of remote controlling.

- 2) A *linear dynamics loss* (\mathcal{L}_2) enforces the linearity of system state evolution within the latent space over k' time steps, as shown as follows.

$$\mathcal{L}_2 = \frac{1}{K_s} \sum_{k=1}^{K_s} \|\mathbf{z}_{k+k'} - \mathbf{D}_A^{k'} \mathbf{z}_{i,k} + \mathbf{D}_B^{k'} \mathbf{u}_{i,k}\|_2^2. \quad (12)$$

- 3) A *prediction loss* (\mathcal{L}_3) ensures accurate prediction of future system states and is provided as follows.

$$\mathcal{L}_3 = \frac{1}{K_s} \sum_{k=1}^{K_s} \|\mathbf{x}_{k+k'} - \Psi^{-1}(\mathbf{D}_A^{k'} \mathbf{z}_{i,k} + \mathbf{D}_B^{k'} \mathbf{u}_{i,k})\|_2^2. \quad (13)$$

The total loss function combines these three losses with an l_2 regularization term to prevent overfitting, leading to the final optimization problem formulated as.

$$\arg \min_{\mathbf{D}_A, \mathbf{D}_B, \Psi, \Psi^{-1}} \sum_{n=1}^3 c_n \mathcal{L}_n + c_4 \|\mathbf{W}\|_2^2, \quad (14)$$

where c_n are positive real coefficients and \mathbf{W} represents the network weights. During this phase, frequent wireless transmission of system states and their representations is required to solve the optimization problem in (14).

In the second phase starting at time $t = k\tau_o$, after training the DSK model, the sensor transmits state representations $\mathbf{z}_{i,k}$ to the controller, which computes control commands $\mathbf{u}_{i,k}$. The controller predicts future states at time $t = (k+l)\tau_o$ using the DSK model and decoder as

$$\tilde{\mathbf{x}}_{k+l} = \Psi^{-1}(\mathbf{D}_A^l \Psi(\mathbf{x}_{i,k}) + \mathbf{D}_B^l \mathbf{u}_{i,k}), \quad (15)$$

for $l \in \mathbb{Z}_+$. To counter prediction errors from communication noise and system uncertainties, periodic model fine-tuning is required, after which other plants adopt the trained models for their control phases outlined below.

B. Logic Semantic Koopman Model

In this phase, we assume that all plants, except plant i , follow predefined control rules. Plant j (where $j \in \mathcal{I} \setminus i$) operates under control rule φ_j and exhibits different dynamics from plant i . Using the encoder, decoder, and DSK model from plant i , plant j derives an LSK model (represented by matrices $\mathbf{L}_{\varphi_j}^A$ and $\mathbf{L}_{\varphi_j}^B$), which captures the system dynamics under φ_j . The optimization problem for the LSK model is given as

$$\arg \min_{\mathbf{L}_{\varphi_j}^A, \mathbf{L}_{\varphi_j}^B} \frac{1}{K_s} \sum_{k=1}^{K_s} \left\| \mathbf{x}_{i,k} - \Psi^{-1} \left(\mathbf{L}_{\varphi_j}^A \mathbf{D}_A \mathbf{z}_{i,k} + \mathbf{L}_{\varphi_j}^B \mathbf{D}_B \mathbf{u}_{i,k} \right) \right\|_2^2. \quad (16)$$

where $\mathbf{L}_{\varphi_j}^A$ and $\mathbf{L}_{\varphi_j}^B$ represent the Koopman matrices parameterized by the control rules φ_j . Due to challenges in obtaining an analytical solution, deep learning is employed. A new loss function, *logic loss* (\mathcal{L}_4), ensures the state representations follow the control rule φ_j and is given by

$$\mathcal{L}_4 = \text{ReLu}(-\rho(s_{j,k}, \varphi_j)), \quad (17)$$

where $s_{j,k}$ denotes the timed trace signal of first state representations, φ_j is the control rule expressed as an STL formula in the latent space.

To develop the STL formula, we first train a conventional AE for a few epochs, then fine-tune the LSK model using time-series state representations and the predefined STL template. For further details, we refer the reader to [9]. The final training objective combines the four loss functions ($\mathcal{L}_1, \mathcal{L}_2, \mathcal{L}_3, \mathcal{L}_4$) with l_2 regularization to prevent overfitting as follows.

$$\arg \min_{\mathbf{L}_{\varphi_j}^A, \mathbf{L}_{\varphi_j}^B} \sum_{n=1}^4 c'_n \mathcal{L}_n + c'_5 \|\mathbf{W}\|_2^2. \quad (18)$$

Once the LSK model is fully trained, plant j integrates it with the DSK model from plant i to construct its Koopman model and perform remote control operation.

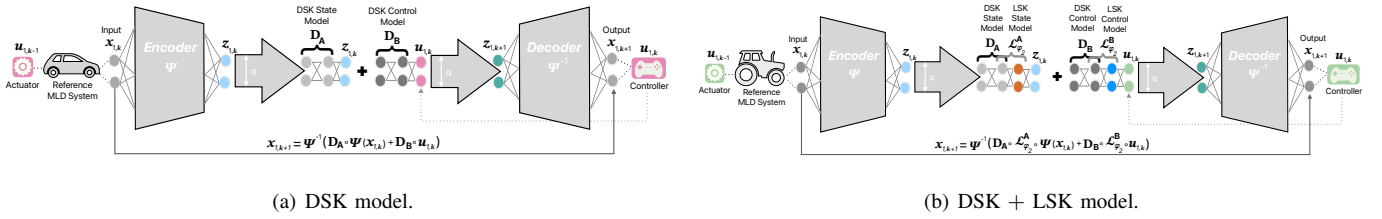


Fig. 2. The logical Koopman AE models for controlling two MLD systems.

IV. SIMULATION RESULTS

This section will validate the proposed logical Koopman AE approach on inverted cart-pole systems over wireless channels. Each system is defined by a four-dimensional state vector representing the horizontal position and velocity of the cart and the vertical angle and angular velocity of the pendulum, and control is applied through a horizontal force. Here, we adopt the following simulation parameter settings unless specified otherwise: the pendulum mass is set to $\{1, 3, 4, 5, 6\}$ Kg, the cart mass is established at $\{5, 15, 20, 25, 30\}$ Kg, and the pendulum length is maintained at $\{0.2, 0.6, 0.8, 1.0, 1.2\}$ m. We simulate five systems with varying parameters, governed by logical control rules, over a temporal span of $[150, 251]$. These logical control rules are defined as

$$\varphi_i := \square_{[151, 251]}((s_{i,k} \geq \beta_i) \wedge (s_{i,k} \leq \beta_i)), \quad (19)$$

for $i \in \{1, 2, 3, 4, 5\}$. The parameter β_i , ranging across $\{0, 2.0, 3.0, 4.0, 5.0\}$, delineates the value within the state space for each respective system. The training data is sampled at a rate of $\tau_0 = 100$ ms over the time interval of $[0, 251]$ and system dynamics are computed using the Runge-Kutta method with a step size of 0.1. The logical Koopman AE model is trained using the Adam optimizer with a batch size of 251, a learning rate of 2×10^{-3} , and early stopping, and experiments are repeated five times with different seeds.

The encoder has a fully connected layer of 32 neurons, activated by a ReLU function, followed by an output layer of $d \in \{2, 4\}$ neurons with sigmoid activation. The decoder mirrors the encoder, while the DSK model includes two fully connected layers, and the LSK model adds two more layers after the DSK matrices are applied. The model is trained with weight hyperparameters $c_1 = 0.1$, $c_4 = 10^{-6}$, and $c_2 = c_3 = 0.75$ for (14), and $c'_1 = 0.1$, $c'_5 = 10^{-6}$, $c'_2 = c'_3 = 0.75$, and $c'_4 = 0.1$ for (18). Wireless performance is evaluated based on SNR values $\gamma_{i,k} \in \{5, 15\}$ dB with a transmission bandwidth (B) of 20 MHz, a path loss exponent (η) of 3.0, a transmission power (P) of 0.1Watt, and the distance between communication pairs (D) of 50m.

The performance is assessed by *sample complexity* (number of communication samples required to train the model) and prediction accuracy using normalized root mean squared error (NRMSE), computed as

$$\mathcal{N}_{i,K_p} = \frac{\sqrt{\frac{1}{K_p} \sum_{k=K_s+1}^{K_s+K_p} \|\tilde{\mathbf{x}}_{i,k} - \mathbf{x}_{i,k}\|_2^2}}{\|\max(\mathbf{x}) - \min(\mathbf{x})\|_2} \times 100, \quad (20)$$

where K_p is the prediction horizon at the test. System stability is measured by a score function that assigns a score of 1 when the cart's position is within 0.2 units of the target location and the pendulum's angle remains within 0.05 radians of the upright position and 0 otherwise. We compare the logical Koopman AE model with two baselines:

- Individual MLD-Koopman model (Baseline 1), where each system has its own AE. Note that the MLD-Koopman model is from our preliminary work [9].
- Shared MLD-Koopman model (Baseline 2) used across all systems.

Impact of Representation Dimensions. Fig. 3 presents the state prediction performance and sample complexity of the proposed logical Koopman AE model with two baseline models, using an SNR of 15 dB, one-step prediction depth, and varying state representation dimensions. The logical Koopman AE model performs similarly to Baseline 1 and significantly outperforms Baseline 2 across all systems. It achieves an NRMSE of about 1% as shown in Fig. 3(a), with the reference system (System 1) reaching 0.2% NRMSE with a four-dimensional representation. Lower-dimensional representations slightly increase the NRMSE to 1.5% as shown in Fig. 3(b), while Baseline 2 shows a much higher 9% error.

The proposed model's success comes from its ability to encode control rules in the latent space via the LSK model, pre-training the encoder and decoder for 50 epochs. The DSK model captures the semantic correlations leveraging reference dynamics, requiring only 10% of the data to encode control rules compared to reference dynamics. By combining DSK and LSK, the model effectively linearizes non-linear dynamics, enabling accurate state predictions with low communication overhead. Note that the encoder and decoder are fine-tuned on systems governed by control rules, enriching the latent space to capture dynamic variations.

Baseline 2, trained only on the reference system, struggles with prediction accuracy, especially with fewer communication samples, due to its inability to handle systems governed by different control rules. Fig. 3(a) shows that high-dimensional representations further improve state prediction performance compared to low-dimensional representations by capturing the most critical eigenfunctions of the system dynamics and modeling the control rules in the latent space. Baseline 1 also benefits from a larger representation dimension, improving Koopman matrix modeling to predict future states at the cost of increased communication overhead. Reducing from four to two-dimensional representations can cut communication samples in half while maintaining reasonable prediction accuracy, hence it is necessary to evaluate control performance under different representation dimensions.

Control Performance. Fig. 4 shows the control performance of the proposed model with two baselines, measured by average score values under different representation dimensions and an SNR of 15 dB. The proposed model closely matches the reference values across all systems, as does Baseline 1, which maintains strong prediction accuracy (around 0.5% NRMSE for four-dimensional and 1% for two-dimensional representations). However, Baseline 2 shows lower state prediction accuracy, impacting its control performance. Despite

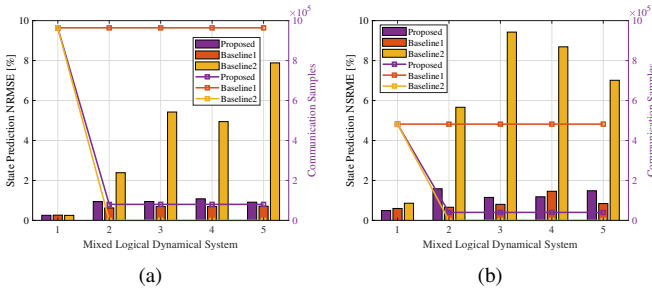


Fig. 3. State prediction and communication samples for each system of proposed and baselines with SNR = 15 dB for (a) $d = 4$ and (b) $d = 2$.

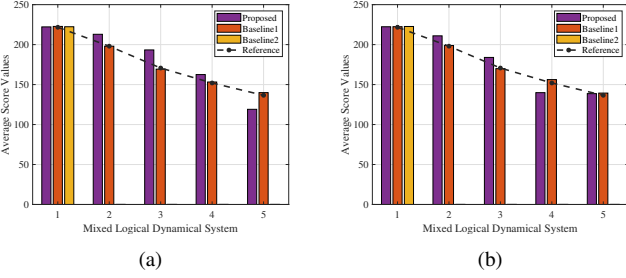


Fig. 4. Average score values for each system of proposed and baselines with SNR = 15 dB for (a) $d = 4$ and (b) $d = 2$.

slight reductions in prediction accuracy with two-dimensional representations shown in Fig. 4(b), the control performance remains nearly unchanged, suggesting that lower-dimensional representations can reduce communication without sacrificing control performance. Average score values tend to decrease for systems further from the reference, as they take longer to reach the target state, leading to slight control performance degradation.

Impact of SNR. Fig. 5 shows the state prediction performance and sample complexity of the proposed model with two baselines across different SNR values using two-dimensional representations and one-step prediction depth. The results indicate that, for both models, state prediction accuracy decreases slightly at lower SNR values compared to higher ones. Both models experience a slight decrease in accuracy at lower SNR values, primarily due to increased packet loss at 5dB, which reduces the training data available. Interestingly, Baseline 1 maintains similar or better performance for systems 4 and 5 at low SNR, likely due to the smaller, more balanced dataset preventing overfitting. In contrast, the proposed model's accuracy declines more significantly at low SNR, likely due to error accumulation in its DSK and LSK components.

V. CONCLUSION

This letter introduces a novel Logical Koopman AE framework designed to manage multi-objective distinct control systems, departing from the previous work that focused on controlling multi-objective identical control systems. The framework integrates two key models: the DSK model, which captures the reference system's semantic structure and linearizes state evolution in the latent space, and the LSK model, which encodes control rules for systems with different control rules and dynamics. Results show that the framework reduces communication overhead for controlling multi-objective distinct dynamics and improves state prediction accuracy without compromising control performance.

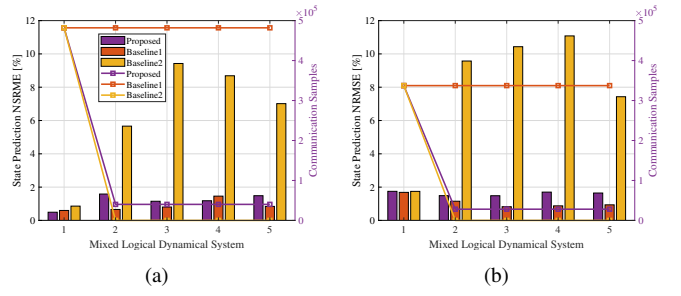


Fig. 5. State prediction and communication samples for each system of proposed and baselines for (a) SNR = 15 dB and (b) SNR = 5 dB.

REFERENCES

- [1] T. Zeng, O. Semiari, W. Saad, and M. Bennis, "Joint communication and control for wireless autonomous vehicular platoon systems," *IEEE Transactions on Communications*, vol. 67, no. 11, pp. 7907–7922, 2019.
- [2] T. M. Getu, G. Kaddoum, and M. Bennis, "A survey on goal-oriented semantic communication: Techniques, challenges, and future directions," *IEEE Access*, 2024.
- [3] A. M. Girgis, J. Park, M. Bennis, and M. Debbah, "Predictive control and communication co-design via two-way Gaussian process regression and AoI-aware scheduling," *IEEE Transactions on Communications*, vol. 69, no. 10, pp. 7077–7093, 2021.
- [4] M. Eisen, S. Shukla, D. Cavalcanti, and A. S. Baxi, "Communication-control co-design in wireless edge industrial systems," in *2022 IEEE 18th International Conference on Factory Communication Systems (WFCS)*. IEEE, 2022, pp. 1–8.
- [5] G. Zhao, M. A. Imran, Z. Pang, Z. Chen, and L. Li, "Toward real-time control in future wireless networks: Communication-control co-design," *IEEE Communications Magazine*, vol. 57, no. 2, pp. 138–144, 2018.
- [6] H. Seo, J. Park, M. Bennis, and M. Debbah, "Semantics-native communication via contextual reasoning," *IEEE Transactions on Cognitive Communications and Networking*, vol. 9, no. 3, pp. 604–617, 2023.
- [7] H. Seo, Y. Kang, M. Bennis, and W. Choi, "Bayesian inverse contextual reasoning for heterogeneous semantics-native communication," *IEEE Transactions on Communications*, vol. 72, no. 2, pp. 830–844, 2024.
- [8] H. Xie, Z. Qin, G. Y. Li, and B.-H. Juang, "Deep learning enabled semantic communication systems," *IEEE Transactions on Signal Processing*, vol. 69, pp. 2663–2675, 2021.
- [9] A. M. Girgis, H. Seo, J. Park, and M. Bennis, "Semantic and logical communication-control co-design for correlated dynamical systems," *IEEE Internet of Things Journal*, 2023.
- [10] S. L. Brunton, B. W. Brunton, J. L. Proctor, and J. N. Kutz, "Koopman invariant subspaces and finite linear representations of nonlinear dynamical systems for control," *PloS one*, vol. 11, no. 2, p. e0150171, 2016.
- [11] K. Leung, N. Aréchiga, and M. Pavone, "Backpropagation for parametric stl," in *2019 IEEE Intelligent Vehicles Symposium (IV)*. IEEE, 2019, pp. 185–192.
- [12] E. Kaiser, J. N. Kutz, and S. L. Brunton, "Data-driven discovery of koopman eigenfunctions for control," *Machine Learning: Science and Technology*, vol. 2, no. 3, p. 035023, 2021.
- [13] J. L. Proctor, S. L. Brunton, and J. N. Kutz, "Generalizing Koopman theory to allow for inputs and control," *SIAM Journal on Applied Dynamical Systems*, vol. 17, no. 1, pp. 909–930, 2018.
- [14] G. Mamakoukas, M. Castano, X. Tan, and T. Murphey, "Local koopman operators for data-driven control of robotic systems," in *Robotics: science and systems*, 2019.
- [15] K. Leung, N. Aréchiga, and M. Pavone, "Back-propagation through signal temporal logic specifications: Infusing logical structure into gradient-based methods," in *International Workshop on the Algorithmic Foundations of Robotics*. Springer, 2020, pp. 432–449.
- [16] R. Zhang, J. Han, A. Zhou, X. Hu, S. Yan, P. Lu, H. Li, P. Gao, and Y. Qiao, "Llama-adapter: Efficient fine-tuning of language models with zero-init attention," *arXiv preprint arXiv:2303.16199*, 2023.